Towards an FEM Approach to Radial Resistance Prediction in Solder-Impregnated HTS Coils

Raymond Hu, Emily-Kei Brewerton, Sriharsha Venuturumilli *Member, IEEE* Konstantinos Bouloukakis, Kris Chappell, Nancy Zhou *Member, IEEE*, Xiyong Huang, Rodney A. Badcock *Senior Member, IEEE*, Ratu C. Mataira

***Abstract*—Solder-impregnated high-temperature superconducting (HTS) coils inherit challenges in predicting the coil characteristics due to their complex radial resistive pathways. Unlike insulated magnets, which require active quench protection and management schemes, non-insulated (NI) coils benefit from inherent quench tolerance through radial current bypass, but require advanced thermal-electrical models to predict charging time-constants and quench-tolerant performance under designed operating regimes.**

This research advances the electrical resistivity characterization of solder alloys at cryogenic temperatures, improving modeling predictions of coil properties. This paper will showcase the methodology utilized for characterizing low-temperature solder alloys, such as InBi, InSn, BiSnAg, and InAg, which enable solder-impregnation at lower reflow temperatures, therefore minimizing tape degradation. Experimental characterization data are validated against existing studies of SnPb solder.

Solder characterization data are incorporated into finite element method (FEM) models to accurately describe temperature-dependent electrical resistivity characteristics between tape turns; thus, by ignoring the HTS layer to be insulating, together with temperature-dependent parameters, the radial resistance of coil 1A is evaluated from the model and compared against the experimental results.

This work enhanced the understanding of solder-impregnated HTS coils, determining the design process of our future magnet systems.

***Index Terms*—Solder-impregnated coils, cryogenic solder, NI coils, HTS Magnets**

I. Introduction

OPENSTAR Technologies implements REBCO coated conductor technologies to realize a magnetic confinement fusion energy system [1]. In particular, a Levitated Dipole concept [2], investigated in the Levitated Dipole Experiment (LDX) [3] and the Ring Trap 1 (RT-1) experiment [4], has been designed using high-temperature superconductor (HTS) technology. The Junior Core Magnet is a 1.44 kA, 5.7 T system comprising of 14 NI solder-impregnated HTS coils connected in series. Solder-impregnated NI coils feature complex thermal and electrical pathways [5], [6]. They offer inherent quench tolerance [7]–[10] through radial current redistribution, eliminating the need for active protection circuits required in insulated coils.

This work was funded by OpenStar Technologies Ltd. (Corresponding author: Raymond Hu.)

Raymond Hu, Emily-Kei Brewerton, Sriharsha Venuturumilli, Konstantinos. Bouloukakis, Kris Chappell, Nancy Zhou, Rodney A. Badcock and Ratu C. Mataira are with OpenStar Technologies, Wellington 6035, New Zealand. (e-mail: raymond.hu@openstar.nz). Rodney A. Badcock is also with Dodd-Walls Centre for Photonic and Quantum Technology, Lower Hutt 5046, New Zealand and Robinson Research Institute, Victoria University of Wellington, Lower Hutt 5046, New Zealand

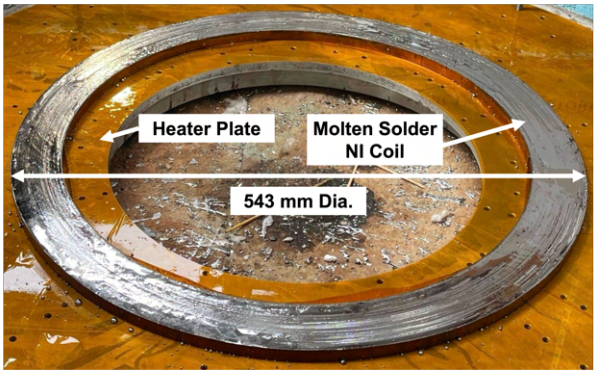

Fig. 1: An OpenStar 543 mm diameter non-insulated solder-impregnated coil; shown in a molten solder state sitting on the hot-plate.

This additional level of complexity in NI coils limits existing modeling approaches to rely on empirical experimental measurements of characteristic resistance [11], [12] to estimate radial resistance. This is typically achieved by measuring small test coils to parametrize equivalent circuit models [8], which are then scaled to full-sized coils with identical parameters including winding tension, strand composition (parallel HTS tapes and stainless-steel co-wind [13], [14]) and tape specification.

This approach misrepresents turn-to-turn contact resistance in NI solder-impregnated coils by defining it as the inter-turn electrical pathway between tape faces, while in practice, radial bypass primarily occurs through the conductive copper edges of HTS tapes [15]. Removing NI solder-impregnated coil faces, and hence the radial bypass, has been demonstrated to fully transform into insulated coils, invalidating contact resistance models predicated on turn-to-turn contact resistive interfaces [16]. Instead, solder on the coil faces forms a surface shunt where the uniformity and thickness determine the turn-to-turn resistance [17], posing a key limitation for accurate modeling of experimental coils. Fig. 1 illustrates this limitation through the coil wetting issues producing non-uniform solder distribution on the face of the coil.

Post-fabrication modeling validates coil performance after construction [8], but cannot guide design decisions prior to fabrication. This limits its value for developing magnets to meet charge time requirements, as designers cannot predict whether a proposed geometry or material combination will meet targets before committing to the manufacturing of coil prototypes.

Unlike empirical methods, this work demonstrates an alternative method of enabling design-phase optimization by predicting radial resistance using bulk material properties alone, eliminating prototype testing during design iteration. This paper provides a comprehensive bulk electrical resistivity characterization database for NI solder-impregnated coil materials, including the copper stabilizer, stainless steel co-wind, and previously uncharacterized 57Bi42Sn1Ag solder, measured across cryogenic temperatures is presented.

To reduce the cost and time associated with winding multiple test coils to achieve a statistically meaningful validation dataset for finite element method (FEM) predictions of radial resistance, an extensive lap joint study was conducted to determine the predictability of FEA models using purely bulk electrical resistivity to describe the electrical behavior occurring in joints [18]. The lap joint samples are geometrically representative of inter-turn segments in full-scale NI coils. The work is subsequently extended by scaling the lap-joint models to full-size solder-impregnated NI coil models, and the resulting prediction accuracy is evaluated against experimental data.

II. Experimental Details

A. Determining Solder Alloy Resistivities

The resistivity of the solder types were measured using a Quantum Design Physical Property Measurement System (PPMS) [19]. Samples of the different solder alloys were mounted onto a standard puck [20] as shown in Fig. 2. Drawn solder alloy wire was wound into a non-inductive spiral using a 3D-printed jig to increase the sample length while minimising the bending radius within the constrained mounting area in Fig. 2a. The sample was soldered to the puck using the matching solder alloy (one wire to V+/I+, the other to V-/I-, then coated with GE-7031 varnish for thermal contact as shown in Fig. 2b).

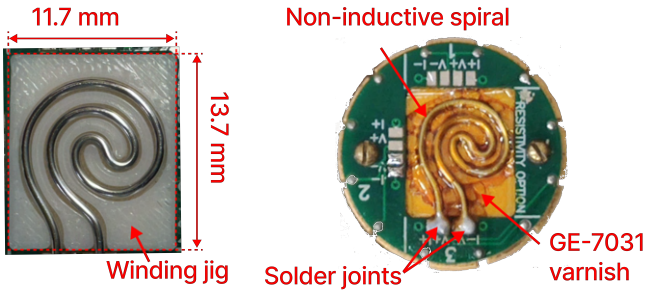

Fig. 2: Process of (a) preparing, (b) soldering, and (c) mounting sample for electrical resistivity characterization

Measurements as shown in Fig. 3 were conducted for six different solder alloys commonly used for HTS applications: 66.3In33.7Bi, 52In48Sn, 57Bi42Sn1Ag, 97In3Ag, 99.999In, and 63Sn37Pb.

The resistivity measurements for 66.3In33.7Bi, 52In48Sn, 99.999In, and 63Sn37Pb, solder agree with existing literature [21]–[23] (note that 57Bi42Sn1Ag and 97In3Ag have not been characterized in prior research, but behaves similarly to the low and high resistivity solders in Fig. 3).

Solder alloys can be classified into two categories: high and low electrical resistivity solder alloys. 52In48Sn, 57Bi42Sn1Ag, and 66.3In33.7Bi solder alloys fall into the high resistivity category, as their electrical resistivities do not decrease exponentially below 100 K (Red patch in Fig 3). These alloys can increase radial resistance in solder-impregnated NI coils and thus shorten their charging time constants ($\tau = L/R$). In contrast, low resistivity solder alloys: 99.999In, 97In3Ag, and 63Sn37Pb show an exponential decrease in electrical resistivity at temperatures below 100K (Blue patch in Fig 3) and are preferred for producing low-resistance tape joints.

As a result, the high resistivity solder alloys are ideal for the coils developed at OpenStar Technologies, where high-field magnets require faster energization to enable frequent plasma confinement cycles. For OpenStar Technologies, magnets use 57Bi42Sn1Ag solder to meet the desired charging time requirement of <2 days when energized by HTS rectifiers (also known as flux pumps [24], [25]), thereby minimizing the turnaround time in experimental campaigns [26]–[28].

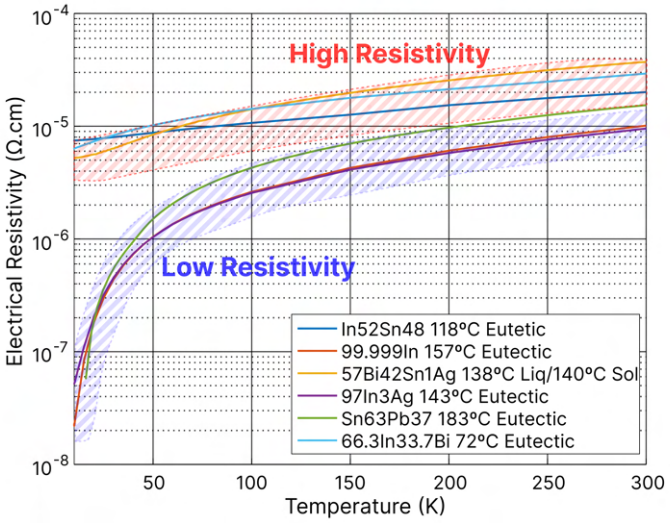

Fig. 3: Bulk electrical resistivity of common solder alloys used in HTS applications

B. Lap Joint Fabrication

Two 200 mm × 12 mm wide "HERMES" HTS tapes supplied by Faraday Factory [29] were used for each lap joint, which was cut to length using a guillotine. The joint length was set to 30 mm, where this section was pre-tinned on the REBCO face of the HTS tapes.

The following hardware in Fig. 4 is used for manufacturing HTS lap solder joints under controlled applied soldering pressure and temperature. This included a PID temperature controller connected to a heater block covering the lap joint, and with a pneumatic actuator applying pressure to the block over the lap joint. The soldering pressure and temperatures were set according to the parameters in Table I. All the samples

discussed in this paper were set to 1.39 MPa of applied soldering pressure as it represents the soldering pressures experienced when fabricating NI solder-impregnated coils at OpenStar Technologies. The heating duration was determined by visual inspection: once excess molten solder extruded from the lap joint, heating was stopped and pressure was maintained until solidification.

Table I outlines the solder alloys tested for average resistance across five repeated samples for each alloy

TABLE I: Fabrication parameters of HTS lap joint samples: sample groups, compositions, applied soldering pressures (P, MPa), alloy liquidus temperature (T_l,°C), heater set-point temperatures (T_H,°C).

Sample	Alloy	P (MPa)	T_l (°C)	T_H (°C)
A1 to A5	66.3In33.7Bi	1.387	72	92
B1 to B5	57Bi42Sn1Ag	1.387	138	158
C1 to C5	97In3Ag	1.387	143	163
D1 to D5	99.999In	1.387	157	177
E1 to E5	63Sn37Pb	1.387	183	203

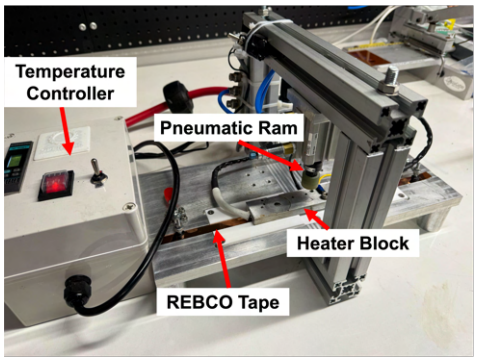

Fig. 4: Hardware for manufacturing HTS lap solder joints under controlled applied soldering pressure and temperature. This includes the temperature controller, heater block, and pneumatic ram assembly.

C. Measuring Lap Joint Resistances

The jig measures HTS lap joint resistance at 77 K using the four-wire Kelvin method [30]–[32] when submerged in LN_2 for accurate cryogenic testing (see Fig. 5). Five identical tape samples per batch are mounted in parallel on the copper bus terminals (see Table I for each sample group) – each sample tested independently by rewiring the power supply negative lead to their corresponding sample. The lead cables on the right-hand side of Fig. 5 are manually disconnected for samples not under test, so only the selected sample remains electrically connected to the current supply. This prevents parallel current paths through the other mounted samples and ensures the measured voltage corresponds to the sample being tested.

The ends of the tapes were soldered onto the copper bus terminals of the jig for I+/I- using 66.3In33.7Bi solder. Voltage taps for V+/V- were then soldered using 63Sn37Pb onto the tapes on either side of the joint, on the REBCO face, and across the entire width of the tape at a spacing of 200 mm.

D. Lap Joint Simulations

A 3D FEM model was constructed in COMSOL® Multiphysics [33] to predict the resistance of the lap joints. The

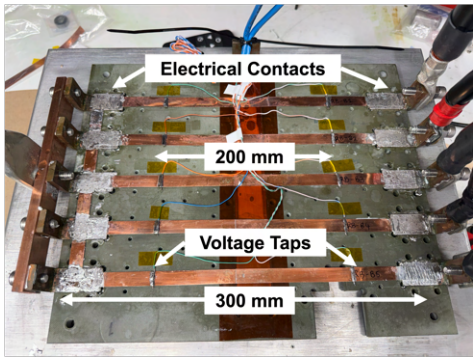

Fig. 5: Joint resistance measurement jig showing five 12 mm wide Faraday Factory superconducting tape lap joints prior to testing in LN_2.

geometry is shown in Fig. 6. To save computation time, the HTS tapes modelled only consist of the layers that are in contact with the solder up until the REBCO, as it is assumed that these are the only layers through which the current passes through. The Electric Currents module was used, with terminal and ground applied to the end faces of the bottom and top tapes, respectively, and the bulk resistivity results from Fig. 3 at 77 K were used as the electrical resistivity of the solder layer.

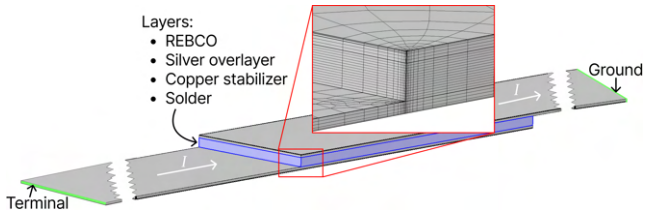

Fig. 6: COMSOL model of lap with inset showing the current path and meshing structure of the joint.The end faces where terminal and ground are set are highlighted in green.

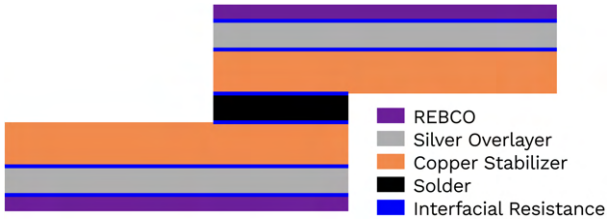

Fig. 7: Sideview of the COMSOL lap joint model (not to scale), showing the different layers, and surfaces where interfacial resistance was added.

The thicknesses of the layers were scaled up by a factor of 20 to help further reduce computation time [34]. As a result, the resistivities of the materials were scaled down by a factor of 20, following the formula [18]:

$$\rho_{\text{actual}} t_{\text{actual}} = \rho_{\text{model}} t_{\text{model}} \tag{1}$$

The experimental and scaled dimensions used in the model are shown in Table II. The experimental thicknesses of the HTS tape layers were taken from the tape manufacturer's

data sheets, and the average solder thicknesses were measured using a micrometer. Interfacial resistances were included between the layers (see Fig. 7) by applying the "Contact Impedance" boundary condition under the "Physics toolbar" in COMSOL, and using the interfacial resistivities from previous work [18].

TABLE II: Dimensions and resistivities of the layers in the lap joint. Resistivities in the "Experimental" column are the values at 77 K.

Variable	Experimental	Model (scaled)
Tape Width	1.2×10^{-2} m	1.2×10^{-2} m
t_{REBCO}	1.0×10^{-6} m	2.0×10^{-5} m
t_{Ag}	2.0×10^{-6} m	4.0×10^{-5} m
t_{Cu}	1.0×10^{-5} m	2.0×10^{-4} m
Average t_{63Sn37Pb}	4.78×10^{-5} m	9.56×10^{-4} m
Average t_{97In3Ag}	3.54×10^{-5} m	7.08×10^{-4} m
Average $t_{\text{99.99In}}$	5.48×10^{-5} m	10.96×10^{-4} m
Average $t_{\text{57Bi42Sn1Ag}}$	4.74×10^{-5} m	9.48×10^{-4} m
Average t_{66In33Bi}	4.06×10^{-5} m	8.12×10^{-4} m
ρ_{REBCO}	N/A	1.0×10^{-18} Ωm
ρ_{Ag}	3.0×10^{-9} Ωm	1.5×10^{-10} Ωm
ρ_{Cu}	4.0×10^{-9} Ωm	2.0×10^{-10} Ωm
ρ_{63Sn37Pb}	3.12×10^{-8} Ωm	1.56×10^{-9} Ωm
ρ_{97In3Ag}	1.88×10^{-8} Ωm	9.41×10^{-10} Ωm
$\rho_{\text{99.99In}}$	1.91×10^{-8} Ωm	9.55×10^{-10} Ωm
$\rho_{\text{57Bi42Sn1Ag}}$	1.16×10^{-7} Ωm	5.78×10^{-9} Ωm
ρ_{66In33Bi}	1.25×10^{-7} Ωm	6.24×10^{-9} Ωm

III. Lap Joint Experiment Results

A. Lap-joint model predictions against experimental data

The experimental results for the lap-joint resistances are shown in Fig. 8 and are compared to model predictions with varying degrees of contact resistivity implementation. The "Model Result A" data points are calculated after applying interfacial resistances to each face between the layers. The "Model Result B" data points are calculated with interfacial resistances added only on the interfaces between the solder and stabilizer layers, and the "Model Result C" data points are calculated with no interfacial resistances at all, using only the bulk resistivities of the materials (assuming perfect contact between layers). It can be seen that 63Sn37Pb solder had the lowest spread in contact resistance, and potentially the lowest joint resistance in measurements of joints. The InAg solder should have the lowest resistivity, but in practice it gave a large variation in lap joints; the spread seen in measurements for all the Bi and In based solders could be due to wetting variation. It is worth noting that the modelled resistance shows a similar trend to the measurements, with the difference expected to be due to contact variations and potentially the interfacial resistivity at the REBCO/silver interface [35].

Fig. 8 reveals that models based solely on bulk solder resistivity and neglecting interfacial resistances consistently underpredict joint resistances across all five alloys. Incorporating contact impedances at tape layers and solder-tape interfaces progressively aligns predictions with experiments, most evidently for In and Bi-based solders, where wettability variations dominate. This refinement bring model predictions closer to experimental error bars. Models using bulk resistivity data alone achieve predictions of the same order of magnitude as experimental measurements. To obtain higher prediction accuracies, models require additional implementations of contact impedance.

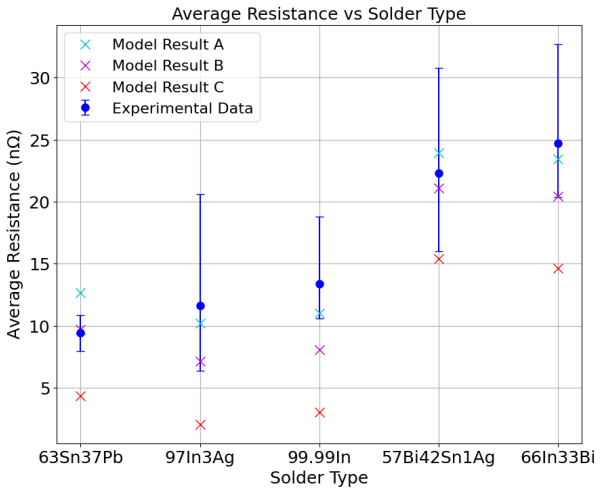

Fig. 8: Experimental data compared to different types model predictions, accounting for pure bulk resisitivity, only HTS contact and all contact resistances.

IV. NI Solder-Impregnated Coil

The lap joint studies in Sections II and III provide key insights into the predictability of joint resistance using FEA models based solely on bulk electrical resistivity data from solder alloys, without explicit interfacial resistivities. These small-scale lap joints represent segments of the turn-to-turn radial pathways in larger solder-impregnated NI HTS coils, enabling scalable modeling that is more efficient than fabricating numerous full coils for predicting radial resistance.

Coil 1A was one of the coils built to be assembled into the Junior Core Magnet. The following radial resistance test was conducted on Coil 1A at 77 K in LN_2.

Coil 1A (see Fig. 1) comprises of four continuous parallel strands of untinned HTS tapes, co-wound in parallel with two stainless-steel tape strands for increasing inter-turn resistance [13], [36], [37]. The coil was wet-wound using 57Bi42Sn1Ag solder paste and reflowed via vacuum-oven solder impregnation to fill inter-turn spaces, ensuring continuous radial pathways.

A. Radial Resistance Testing

Testing the coil involved cooling it to 100 K with gaseous N_2 at a rate of 1 K/min to prevent thermal shock, then submerging it in LN_2. Following cooling, an input step current of 20 A was applied at a rate of 0.2 A/ms using a TDK Lambda GSP10-1500 [38]. A Keithley 2182A Nanovolt meter [39] was used to measure the coil voltage and the radial resistance of the coil was calculated using Ohm's Law [16]. Several resistance measurements were also taken during the gaseous cooling stage using a step current of 5 A. A Lakeshore 224 [40] and Zirnox [41] cryogenic temperature sensors was used to monitor the coil temperature.

B. NI Solder-Impregnated Coil Model Predictions Against Experimental Data

A 2D axisymmetric model was developed in COMSOL, again using the Electric Currents module, to predict the radial resistance of Coil 1A, as seen in Fig. 9. Each turn of the coil was constructed to match the winding process and includes separate geometries for each of the tapes, both stainless steel and HTS, as well as separate geometries for the Hastelloy substrate, Silver overlayer, REBCO, and Copper stabilizer layers within the HTS tape. The REBCO layers were assigned a resistivity of 1 Ωm, to ensure the current passes primarily through the remaining layers within the HTS tapes. The electrical resistivities of the remaining layers are the same as the values listed in the "Experimental" column of Table II. The Contact Impedance boundary condition was not applied to the interfaces to reduce computation time, and because reliable contact resistivity values for the specific material pairings and surface conditions used were not available. Experimental

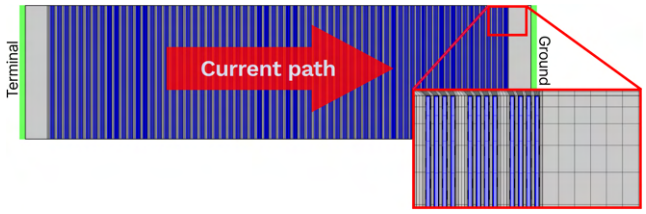

Fig. 9: Coil 1A FEA Model, showing the cross-section view of the solder-impregnated REBCO tapes and solder between. The edges where terminal and ground are applied are highlighted in green.

results from Coil 1A's radial resistance measurements are compared with the model predictions using bulk resistivity data.

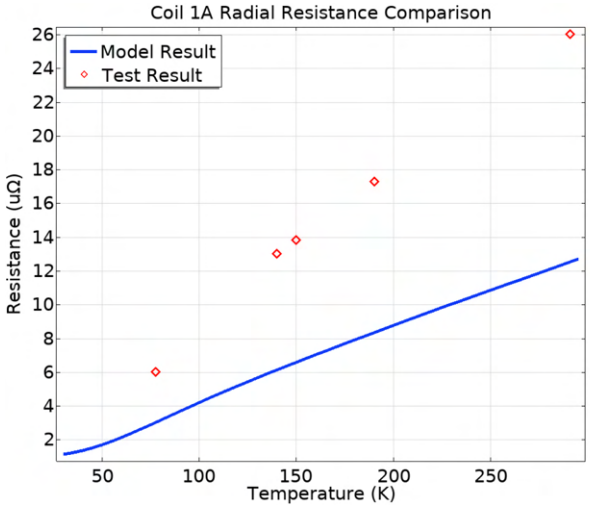

Fig. 10: Coil 1A experimental result against FEA model prediction using only bulk-resistivity data.

The model captures the expected monotonic increase in resistance with temperature; however, the experimental values are systematically higher than the modelled values at all measured points, and the magnitude of the discrepancy grows with temperature. This bias is consistent with the simplifying assumption in the model that neglected electrical contact resistance between turns of the coil. The increasing divergence at higher temperature suggests that contact resistance is not constant with temperature, potentially due to thermally driven changes in contact microstructure, differential thermal expansion, or evolving interface conductivity.

Similar to the prediction behavior of lap solder joints in Fig. 8, modeling Coil 1A purely with bulk electrical resistivity data under-predicts the measured radial resistance, but achieves the same order of magnitude. It further supports the need for creating an extensive database of interfacial contact resistivities to refine this method of predicting joint resistance.

At 77 K, the radial resistance of Coil 1A was measured to be 6.02 $\mu\Omega$. In standardised units, this corresponds to 16.70 $\mu\Omega$ cm^2. This value is consistent with prior reported measurements for comparable NI coils at 77 K [42], suggesting that Coil 1A exhibits typical inter-turn electrical behaviour.

V. Conclusions

This paper for the first time presented novel design-phase modeling techniques aimed towards predicting the radial resistance of solder-impregnated HTS coils. This proposed method challenges all previous studies based on experimental results, requiring prototype coils for any change to the coil design or manufacturing process.

It is assumed that the radial resistance of the coils arises primarily from the bulk resistivity of all materials along the radial current path. This physics is the same as for lap joint resistance. Thus, lap joints are used for model verification, mainly because they enable the generation of a large experimental dataset, thereby reducing error. Characterisation data for solders are fundamental for predicting joint and radial resistances; a comprehensive dataset was measured using the Quantum Design PPMS.

The lap joint resistance measurements indicated a large variation, signifying the dataset size being crucial and sensitivity to the sample fabrication process. Nevertheless, models that use bulk resistivity alone consistently underpredicted the experimental values. Inspired by literature, upon considering contact resistances in the model, both results demonstrated convergence towards experimental results. This concluded that contact resistance is a real phenomenon that cannot be ignored when predicting joint resistances.

Unlike lap joint resistance, the radial resistive path in the non-insulated solder impregnated coils consists of several interfaces, for which data for the distinct interfacial contact resistivities were unavailable. Considering this limitation, an attempt is made to predict the radial resistance with bulk resistivity alone. Similar to lap joint resistance, the modelling results are shown to underpredict the experimental values. Nevertheless, the models can predict to within the same order of magnitude ($\mu\Omega$) as the experimental results, indicating that the approach is physically reasonable for predicting the radial resistance.

Any future work requires the characterisation of all electrical interfaces within the coil, and a larger dataset of radial resistance measurements to quantify the deviation.

REFERENCES

[1] C. S. Chisholm, T. Berry, D. T. Garnier, R. A. Badcock *et al.*, "Design and initial results from the "junior" levitated dipole experiment," *Fusion Engineering and Design*, 2025, DOI:10.1016/j.fusengdes.2025.114746.

[2] A. Hasegawa, L. Chen, and M. E. Mauel, "A d-3he fusion reactor based on a dipole magnetic field," *Nuclear Fusion*, vol. 30, no. 11, pp. 2405–2413, 1990, DOI:10.1088/0029-5515/30/11/018.

[3] D. T. Garnier, A. Hansen, M. E. Mauel, E. Ortiz, A. C. Boxer, J. Ellsworth, I. Karim, J. Kesner, S. Mahar, and A. Roach, "Production and study of high-beta plasma confined by a superconducting dipole magnet," *Physics of Plasmas*, vol. 13, no. 5, p. 056111, may 2006, DOI:10.1063/1.2186616.

[4] J. Morikawa *et al.*, "Development of a super-conducting levitated coil system in the rt-1 magnetospheric confinement device," *Fusion Engineering and Design*, vol. 82, no. 5–14, pp. 1437–1442, oct 2007, DOI:10.1016/j.fusengdes.2007.03.050.

[5] S. Hahn, D. K. Park, J. Bascunan, and Y. Iwasa, "Hts pancake coils without turn-to-turn insulation," *IEEE Transactions on Applied Superconductivity*, vol. 21, no. 3, pp. 1592–1595, 2011, DOI:10.1109/TASC.2010.2093492.

[6] Y. Li *et al.*, "Feasibility study of the impregnation of a no-insulation hts coil using solder," *IEEE Transactions on Applied Superconductivity*, vol. 28, no. 1, pp. 1–5, 2018, DOI:10.1109/TASC.2017.2773831.

[7] Y. Wang, W. K. Chan, and J. Schwartz, "Self-protection mechanisms in no-insulation (RE)$Ba_2Cu_3O_x$ high temperature superconductor pancake coils," *Superconductor Science and Technology*, vol. 29, no. 4, p. 045007, apr 2016, DOI:10.1088/0953-2048/29/4/045007.

[8] X. Wang *et al.*, "Turn-to-turn contact characteristics for an equivalent circuit model of no-insulation ReBCO pancake coil," *Superconductor Science and Technology*, vol. 26, no. 3, p. 035012, 2013, DOI:10.1088/0953-2048/26/3/035012.

[9] S. Hahn, D. K. Park, K. Kim, J. Bascuñán, and Y. Iwasa, "No-insulation (NI) winding technique for premature-quench-free NbTi MRI magnets," *IEEE Transactions on Applied Superconductivity*, vol. 22, no. 3, p. 4501004, December 2011, DOI:10.1109/TASC.2011.2178970.

[10] S. Hahn, "No-insulation winding technique for high temperature superconductor (hts) magnets," *Journal of Cryogenics and Superconductivity Society of Japan*, vol. 53, no. 1, pp. 2–11, 2018, DOI:10.4191/kcse.53.2.

[11] J. Olatunji, H. Weijers, N. Strickland, and S. Wimbush, "Modelling the quench behavior of an ni hts applied-field module for a magnetoplasmadynamic thruster undergoing a 1kw discharge," *IEEE Transactions on Applied Superconductivity*, vol. 33, no. 5, 2023, DOI:10.1109/TASC.2023.3264170.

[12] S. Venuturumilli, R. C. Mataira, R. W. Taylor, J. T. Gonzales, and C. W. Bumby, "Modeling HTS non-insulated coils: A comparison between finite-element and distributed network models," *AIP Advances*, vol. 13, no. 3, p. 035317, mar 2023, DOI:10.1063/5.0135291.

[13] C. Li *et al.*, "The investigation on the turn-to-turn contact resistivity of REBCO co-wound with stainless steel and hastelloy," *Physica C: Superconductivity and its Applications*, vol. 636, p. 1354769, 2025, DOI:10.1016/j.physc.2025.1354769.

[14] J. Kim, D. Park, F. Dong, A. Lanzrath, W. Lee, J. Bascuñán, and Y. Iwasa, "Self-protection characteristic comparison between no-insulation, metal-as-insulation, and surface-shunted-metal-as-insulation REBCO coils," *IEEE Transactions on Applied Superconductivity*, vol. 33, no. 5, p. 4603105, 2023, DOI:10.1109/TASC.2023.3267727.

[15] T. Mulder *et al.*, "Method of manufacturing fast ramping non-insulated HTS pancake coils," Presented at MT27 (WED-OR2-703-04), November 2021, 17.

[16] S. Venuturumilli, "Hts magnet technology," Presentation at EFATS Conference, IEEE CSC & ESAS Superconductivity NewsForum (global edition), August 2022, presented 30–31 August 2022, Glasgow, UK. [Online]. Available: https://snf.ieeecsc.org/files/ieeecsc/slides/Venturumilli%20presentation%20final.pdf

[17] W. Lee *et al.*, "Construction and test result of an all-rebco conduction-cooled 23.5 t magnet prototype towards a benchtop 1 ghz nmr spectroscopy," *Superconductor Science and Technology*, vol. 35, no. 10, p. 105007, 2022, DOI:10.1088/1361-6668/ac8773.

[18] Z. Huang, Y. Tan, R. He, Y. Xie, G. Wang, J. Wei, Y. Wang, and Q. Wu, "Study on the electrical performances of soldered joints between hts coated-conductors," *Cryogenics*, vol. 122, p. 103422, 2022, DOI:10.1016/j.cryogenics.2022.103422.

[19] Q. Design, "Physical property measurement system (ppms)," https://qdusa.com/products/ppms.html, 2025, october, 2025.

[20] Quantum Design, *DC Resistivity Option for DynaCool (D400), PPMS (P400), VersaLab (V400)*, Quantum Design Inc., 2022, product brochure, revision D0.

[21] Y. Tsui, E. Surrey, and D. Hampshire, "Soldered joints—an essential component of demountable high temperature superconducting fusion magnets," *Superconductor Science and Technology*, vol. 29, no. 7, p. 075005, may 2016, DOI:10.1088/0953-2048/29/7/075005.

[22] N. Bagrets, C. Barth, and K.-P. Weiss, "Low temperature thermal and thermo-mechanical properties of soft solders for superconducting applications," *IEEE Transactions on Applied Superconductivity*, vol. 24, no. 3, pp. 1–3, 2014, DOI:10.1109/TASC.2013.2283869.

[23] L. A. Hall, "Survey of electrical resistivity measurements on 16 pure metals in the temperature range 0 to 273 °k," Gaithersburg, MD, 1968, 107 pages.

[24] B. Leuw *et al.*, "Progress toward a 10-ka superconducting power supply for levitated dipole reactors," *IEEE Transactions on Applied Superconductivity*, 2025, 10.1109/TASC.2026.3654477.

[25] J. Ma *et al.*, "High-temperature superconducting (hts) transformer-rectifier flux pump for powering no-insulation superconducting magnet with low characteristic resistance," *Physica C: Superconductivity and its Applications*, vol. 560, pp. 1–6, 2019, DOI:10.1016/j.physc.2019.01.013.

[26] R. Mataira, M. D. Ainslie, R. Badcock, and C. W. Bumby, "Modelling parallel-connected, no-insulation high-t_c superconducting magnets," *IEEE Transactions on Applied Superconductivity*, vol. 31, no. 5, pp. 1–5, 2021, DOI:10.1109/TASC.2021.3065284.

[27] J. Ma *et al.*, "Flux pumping for non-insulated and metal-insulated hts coils: the effects of parallel-connected secondaries," *Superconductor Science and Technology*, vol. 31, no. 1, p. 015018, 2018, DOI:10.1088/1361-6668/aa99f2.

[28] J. Chen *et al.*, "Investigation and analysis of turn-to-turn contact resistance of a no-insulation ybco pancake coil under time-varying," *Physica C: Superconductivity and its Applications*, vol. 576, p. 1353688, 2020, DOI:10.1016/j.physc.2020.1353688.

[29] F. Factory, "Hts tape for magnets - data book," Faraday Group, Tech. Rep., 2025, accessed: 2025-10-13.

[30] S. L. Lalitha, "Low resistance splices for hts devices and applications," *Cryogenics*, vol. 86, pp. 7–16, 2017, DOI:10.1016/j.cryogenics.2017.06.003.

[31] Y. Chen, P. Zheng, T. Che, W. Qian, X. Chen, S. Jiang, and B. Shen, "Hts joint resistance for high-field magnets: Experiment and temperature-dependent modeling," *Journal of Superconductivity and Novel Magnetism*, vol. 35, no. 7, pp. 1089–1100, 2022, DOI:10.1007/s10948-022-06181-0.

[32] W. S. Marshall, M. Abraimov, J. Lu, and N. Gavin, "Rebco soldered lap joint resistance versus length and tape manufacturer," *IEEE Transactions on Applied Superconductivity*, vol. 35, no. 5, pp. 1–4, 2025, DOI:10.1109/TASC.2024.3499969.

[33] C. Multiphysics, "Introduction to comsol multiphysics®," *COMSOL Multiphysics, Burlington, MA, accessed Feb*, vol. 9, p. 2018, 1998.

[34] Z. Hong and T. Coombs, "Numerical modelling of ac loss in coated conductors by finite element software using h formulation," *Journal of Superconductivity and Novel Magnetism*, vol. 23, no. 8, pp. 1–5, 2010.

[35] Y. Tsui, E. Surrey, and D. Hampshire, "Soldered joints—an essential component of demountable high temperature superconducting fusion magnets," *Superconductor Science and Technology*, vol. 29, no. 7, p. 075005, may 2016, DOI:10.1088/0953-2048/29/7/075005.

[36] T. Lécrevisse, X. Chaud, P. Fazilleau, C. Genot, and J.-B. Song, "Metal-as-insulation hts coils," *Superconductor Science and Technology*, vol. 35, no. 7, p. 074004, may 2022, . [Online]. Available: https://doi.org/10.1088/1361-6668/ac49a5

[37] S. Noguchi *et al.*, "Numerical investigation of metal insulation technique on turn-to-turn contact resistance of rebco pancake coils," *IEEE Transactions on Applied Superconductivity*, vol. 27, no. 4, pp. 1–5, 2017, .

[38] TDK-Lambda Corporation, *GSP10-1500 Programmable DC Power Supply Datasheet*, TDK-Lambda Corporation, Shibaura Renasite Tower, 3-9-1 Shibaura, Minato-ku, Tokyo 108-0023, Japan, 2022, accessed: 2025-10-13. [Online]. Available: https://product.tdk.com/en/search/power/switching-power/prg-power/info?part_no=GSP10-1500-3P400

[39] Keithley Instruments, LLC, *Model 2182A Nanovoltmeter User's Manual*, rev. b ed., Keithley Instruments, LLC, Cleveland, Ohio, USA, 2017, document Number: 2182A-900-01.

[40] Lake Shore Cryotronics, Inc., *Model 224 Temperature Monitor User's Manual*, rev. 1.1 ed., Lake Shore Cryotronics, Inc., 575 McCorkle Blvd., Westerville, Ohio 43082, USA, 2015, p/N 119-062.

[41] Scientific Instruments, Inc., "Zirnox zirconium oxynitride cryogenic temperature sensor," 2022.

[42] Z. Hong and T. Coombs, “Metal-as-insulation hts coils,” *Superconductor Science and Technology*, vol. 35, no. 7, pp. 2–6, 2022.